Subgrid scale modeling taking the numerical error into consideration

By Youhei Morinishi[1] AND Oleg V. Vasilyev[2]

1. Motivation and objectives

Large eddy simulation (LES) is regarded as one of the most promising numerical methods to predict unsteady turbulent flows at high Reynolds number. In LES the flow field is decomposed into grid and subgrid scales. The grid scale (GS) flow field is computed numerically using discrete filtered Navier-Stokes equation with a model for the subgrid scale (SGS) stress. Therefore, the reliability of the computed flow field is strongly affected by both the reliability of the SGS model and the accuracy of the numerical method (Ghosal 1996), particularly in the approximation of the convective term. This means that even if we use the exact SGS stress, the computed flow field will be contaminated by the numerical error. This connection between SGS modeling and numerical error was mostly overlooked. As a result all of the existing SGS models have been developed independently from the numerical methods.

One of the objectives of this study is to develop a dynamic subgrid scale model, for which computational results will not depend on the accuracy of the numerical method. The most commonly used SGS model is based on the Smagorinsky eddy viscosity model (Smagorinsky, 1963) with the model coefficient computed dynamically through the *tensor level* identity by Germano *et al.* (1991), hereafter denoted by DSM. However, the tensor level identity does not explicitly include the effect of the numerical error, and thus the computational results strongly depend on the numerical method, especially in simulations with poor resolution. In this report we will present a new dynamic procedure with the *vector level* identity, which takes the numerical error into consideration. We will test the dynamic Smagorinsky SGS model with the vector level identity, hereafter referred as VDSM model.

The second objective of this study is to present a modification to the dynamic two-parameter mixed model. It is well known that the correlation between the Smagorinsky model and the SGS stress is low (for example see Horiuti 1989) while the model based on the scale similarity assumption by Bardina *et al.* (1983) has considerably higher correlation. However, the scale similarity model has a defect: it is not dissipative enough. Therefore, the model is usually used together with the Smagorinsky model. Model coefficients are commonly computed using the dynamic procedure (Zang *et al.* 1993; Vreman *et al.* 1994; Salvetti & Banerjee 1995; Horiuti

1 Nagoya Institute of Technology, Japan

2 Present address: Department of Mechanical and Aerospace Engineering, University of Missouri, Columbia, MO 65211

1997). Nevertheless, the two-parameter mixed model is still not dissipative enough, and the defect of the scale similarity model is not cured by the dynamic procedure. Recently Morinishi (1997) recommended a modification to the two-parameter dynamic procedure which removes that defect. In this study, we will apply the modification to the dynamic two-parameter mixed model (DTM) of Salvetti and Banerjee (1995) since the model seems to be the standard dynamic two-parameter mixed model. The revised model will be named DTMR.

In this study, all computational tests will be done in the turbulent channel flow, and the Reynolds number based on the channel half width and wall friction velocity is 395. To remove the ambiguity regarding the accuracy of the finite difference scheme, we use the higher (up to 12th) order accurate fully conservative finite difference schemes in a staggered grid system proposed by Morinishi *et al.* (1998).

The present report is organized as follows. In section 2.1 numerical method for the channel flow is outlined and the computational results for channel flow without SGS model is presented as a reference. In section 2.2 the dynamic procedure with the vector level identity is proposed and the computational result of VDSM is compared with those of DSM. In section 2.3 a recommended modification to the dynamic two-parameter mixed model is presented and the the computational result of DTMR is compared with those of DTM.

2. Accomplishments

2.1 Numerical method and no SGS model simulation

The basic LES equations for incompressible flows are the filtered Navier-Stokes and continuity equations given by

$$\frac{\partial \bar{u}_i}{\partial t} + \overline{\frac{\partial u_i u_j}{\partial x_j}} = -\frac{\partial \bar{p}}{\partial x_i} + \nu \frac{\partial^2 \bar{u}_i}{\partial x_j \partial x_j}, \tag{1}$$

$$\frac{\partial \bar{u}_i}{\partial x_i} = 0. \tag{2}$$

Here u_i is the velocity component in x_i direction ($i = 1, 2, 3$), p is the pressure divided by the density, ν is the kinematic viscosity, and t is time. The overbar $\overline{\cdot}$ means filtering operator. The commutability between the differentiation and filtering operations is usually assumed, and the filtered convective term is treated as

$$\overline{\frac{\partial u_i u_j}{\partial x_j}} = \frac{\partial \bar{u}_i \bar{u}_j}{\partial x_j} + \frac{\partial \tau_{ij}}{\partial x_j}, \tag{3}$$

where $\tau_{ij} = \overline{u_i u_j} - \bar{u}_i \bar{u}_j$ is the SGS stress which should be modeled.

In this study the numerical tests of several SGS models, described in the subsequent sections, are performed using fully developed plane channel flow. The flow field is assumed to be periodic in the streamwise (x_1) and spanwise (x_3) directions. The Reynolds number ($Re_\tau = u_\tau h/\nu$) based on the channel half width h and the wall friction velocity u_τ is 395. The treatment of the convective term (the

first term in the right-hand side of Eq. (3)) is important for unsteady turbulent numerical simulations at high Reynolds number. Fully conservative higher (2nd, 4th, 8th and 12th) order accurate finite difference schemes proposed by Morinishi *et al.* (1998) are used for the convective term in the periodic directions. The second order accurate scheme in the wall normal direction (x_2) is combined properly and used in order to remove the ambiguity regarding both the conservation properties of the non-uniform meshes and the wall boundary treatment. A semi-implicit time marching method is used. The diffusion term in the wall normal direction is treated implicitly with the Crank-Nicolson method, and a third order Runge-Kutta (RK3) method of Spalart *et al.* (1991) is used for all other terms. The splitting method by Dukowicz and Dvinsky (1992) is used to enforce the solenoidal condition. The resulting discrete Poisson equation for the pressure is solved using a discrete Fourier transform in the periodic directions and a tri-diagonal direct matrix solver in the wall normal direction. The computational box is $2\pi h \times 2h \times 2\pi h/3$ and $32 \times 64 \times 32$ mesh points are used. The grid spacings in the periodic directions are uniform. In this case, the grid spacings in wall units are $\Delta^+_{x_1} = 77.6$ and $\Delta^+_{x_3} = 25.9$. The wall normal grid is stretched using a hyperbolic-tangent function

$$\frac{x_2(j)}{h} = \frac{\tanh[\gamma(2j/N_2 - 1)]}{\tanh[\gamma]}, \qquad j = 0, \ldots, N_2,$$

where $x_2(j)$ is the wall normal grid point for u_2 in the staggered grid system and $x_2(0)$ and $x_2(64) = x_2(N_2)$ correspond to the lower and upper walls respectively. The stretching parameter, γ, is taken to be 2.75. Time increment is $\Delta t = 2.5 \times 10^{-3}$, and it satisfies the stability condition for RK3. The filtering operations in the dynamic SGS models are done in the periodic directions. The test filtering with the filter width $\hat{\Delta}_1 = 2\Delta_{x_1}$ and the grid filtering with the filter width $\bar{\Delta}_1 = \Delta_{x_1}$ in x_1 direction are done respectively as follows:

$$\hat{f}(x_1) = \frac{1}{6}\big[f(x_1 - \Delta_{x_1}) + 4f(x_1) + f(x_1 + \Delta_{x_1})\big],$$
$$\bar{f}(x_1) = \frac{1}{24}\big[f(x_1 - \Delta_{x_1}) + 22f(x_1) + f(x_1 + \Delta_{x_1})\big].$$

Figures 1 and 2 show the profiles of mean streamwise velocity and velocity fluctuations respectively by the higher order schemes without SGS model at Re_τ=395. In these figures the DNS data by Mansour *et al.* (1996) (see also (Rodi & Mansour 1993)), are also plotted. Note that with the increase of the order of accuracy, the results of finite difference calculations converge. The error of the second order scheme acts as an effective SGS stress, and the mean velocity profile by the second order scheme looks the best on Fig. 1. However, the profile of the velocity fluctuations of the second order scheme is the worst. The differences between the no SGS model simulations and DNS results should be piked up by the SGS model. The amount of required SGS stress depends on the accuracy of the numerical method and the grid resolution.

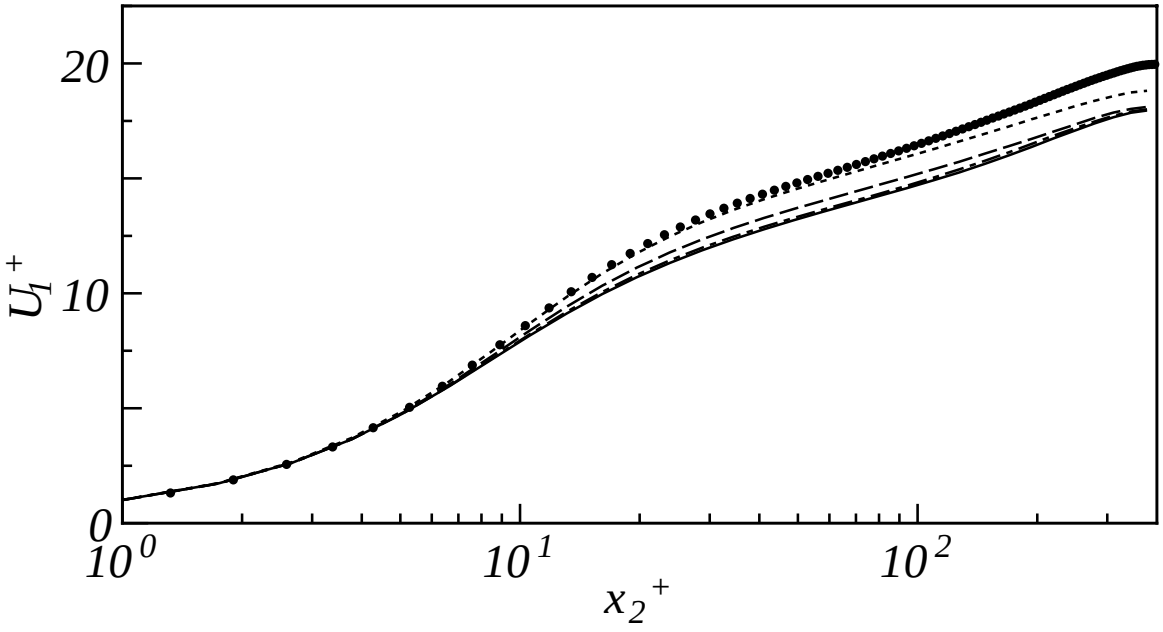

FIGURE 1. Mean streamwise velocity of the channel flow at $Re_\tau = 395$ using no SGS model with the 2nd (·····), 4th (– – – –), 8th (— — —) and 12th (———) order schemes. DNS (•) data are also plotted.

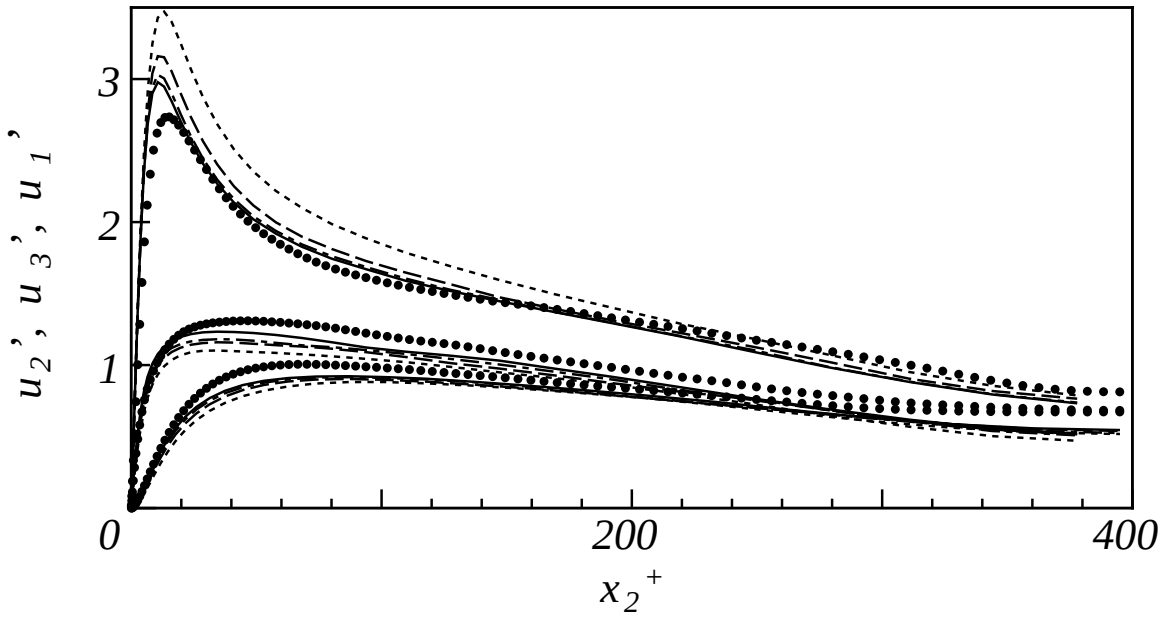

FIGURE 2. Velocity fluctuations of the channel flow at $Re_\tau = 395$ using no SGS model. For symbols see Fig. 1.

2.2 Tensor and vector level identities for the dynamic SGS model

In the dynamic SGS model, the tensor level identity of Germano *et al.* (1991) between the grid and test fields is used to determine the parameter in the SGS model

$$\mathcal{L}_{ij} = T_{ij} - \hat{\tau}_{ij}, \tag{4}$$

where the subtest stress T_{ij} is defined as $T_{ij} = \widehat{\overline{u_i u_j}} - \hat{\bar{u}}_i \hat{\bar{u}}_j$, and the resolved stress $\mathcal{L}_{ij}$ is defined as

$$\mathcal{L}_{ij} = \widehat{\bar{u}_i \bar{u}_j} - \hat{\bar{u}}_i \hat{\bar{u}}_j. \tag{5}$$

The Smagorinsky eddy viscosity model is assumed for both the subgrid and subtest stresses in the standard dynamic SGS model.

$$\tau^*_{ij} = -2(C_S\bar{\Delta})^2|\bar{S}|\bar{S}_{ij}, \qquad \bar{S}_{ij} = \frac{1}{2}\Big(\frac{\partial \bar{u}_i}{\partial x_j} + \frac{\partial \bar{u}_j}{\partial x_i}\Big), \qquad |\bar{S}| = \big(2\bar{S}_{ij}\bar{S}_{ij}\big)^{1/2} \tag{6}$$

$$T^*_{ij} = -2(C_S\hat{\bar{\Delta}})^2|\hat{\bar{S}}|\hat{\bar{S}}_{ij}, \qquad \hat{\bar{S}}_{ij} = \frac{1}{2}\Big(\frac{\partial \hat{\bar{u}}_i}{\partial x_j} + \frac{\partial \hat{\bar{u}}_j}{\partial x_i}\Big), \qquad |\hat{\bar{S}}| = \big(2\hat{\bar{S}}_{ij}\hat{\bar{S}}_{ij}\big)^{1/2} \tag{7}$$

The superscript "*" denotes the trace free operator ($\tau^*_{ij} \equiv \tau_{ij} - \frac{1}{3}\delta_{ij}\tau_{kk}$). The model parameter C_S is computed by minimizing the the square of the error $Q = E_{ij}E_{ij}$ (Lilly, 1992), where the error E_{ij} is given by

$$\begin{aligned} E_{ij} &= \mathcal{L}^*_{ij} + 2(C_S\bar{\Delta})^2 M_{ij}, \\ M_{ij} &= \alpha^2|\hat{\bar{S}}|\hat{\bar{S}}_{ij} - \widehat{|\bar{S}|\bar{S}}_{ij}, \end{aligned} \tag{8}$$

and $\alpha^2 = (\hat{\bar{\Delta}}/\bar{\Delta})^2$ is the square value of the test to grid filter widths ratio. In this study we take $\alpha^2 = 4^{2/3} \sim 2.52$. Assuming C_S is a function of x_2, and taking the average in $x_1 - x_3$ plane (denoted by $\langle\cdot\rangle$), we obtain the following equation for $(C_S\bar{\Delta})^2$:

$$(C_S\bar{\Delta})^2 = -\frac{1}{2}\frac{\langle \mathcal{L}_{ij}M_{ij}\rangle}{\langle M_{ij}M_{ij}\rangle}. \tag{9}$$

In this report the dynamic Smagorinsky model given by Eqs. (6) and (9) is called DSM.

Figures 3, 4, and 5 show the profiles of mean streamwise velocity, velocity fluctuations, and the SGS eddy viscosity respectively using the higher order schemes with DSM at Re_τ=395. The SGS eddy viscosity is defined as $\nu_{\rm t} = (C_S\bar{\Delta})^2|\bar{S}|$. Note that the mean streamwise velocity profiles of the simulations with DSM are shifted up when compared to the results of the simulations without SGS model. The mean velocity and turbulent intensity profiles of DSM do not depend strongly on the order of the accuracy except for the second order scheme. This means that the effect of the numerical error of the second order scheme is considerably larger than those of the higher order schemes. The implicit effect of the order of the finite difference schemes on the eddy viscosity is shown in Fig. 5. The eddy viscosity

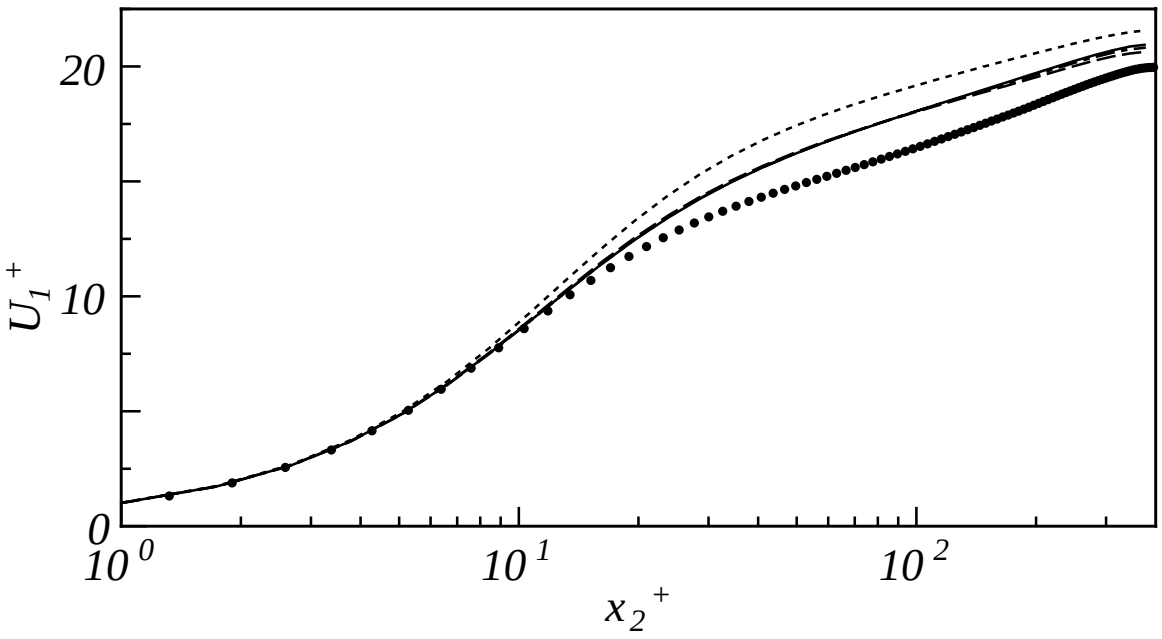

FIGURE 3. Mean streamwise velocity of the channel flow at Re_τ =395 using DSM with the 2nd (·····), 4th (- - - -), 8th (— — —) and 12th (———) order schemes. DNS (•) data are also plotted.

increases gradually with the increase of the order of the scheme. Even for the 12th order scheme, the dynamic procedure with the Smagorinsky model gives excessive SGS eddy viscosity for the chosen resolution, and the mean velocity profile is much higher than the DNS data.

Note that in practical LES applications the finite difference method is usually used, and the first term in the right-hand side of Eq. (3) is approximated by

$$\frac{\partial \bar{u}_i \bar{u}_j}{\partial x_j} = \frac{\delta \bar{u}_i \bar{u}_j}{\delta x_j} + O(h^n), \tag{10}$$

where $\delta u_i u_j / \delta x_j$ is the n-th order accurate finite difference approximation to $\partial u_i u_j / \partial x_j$ and $O(h^n)$ denotes the truncation error. This means that the filtered convective term Eq. (3) suffers from the effect of the numerical error even if we know the exact SGS stress. That is why the development of the higher order accurate finite difference methods has been considered as one of the important areas of LES research.

In this study, we propose an alternate approach to improve the reliability of computational results of LES. The filtered convective term in the grid field is modeled as

$$\overline{\frac{\partial u_i u_j}{\partial x_j}} = \frac{\delta \bar{u}_i \bar{u}_j}{\delta x_j} + \frac{\partial \tau_{ij}}{\partial x_j}, \tag{11}$$

where the numerical error is treated as a part of the SGS stress (exactly, SGS vector) and the rest is modeled with τ_{ij}. The filtered convective term in the test field is

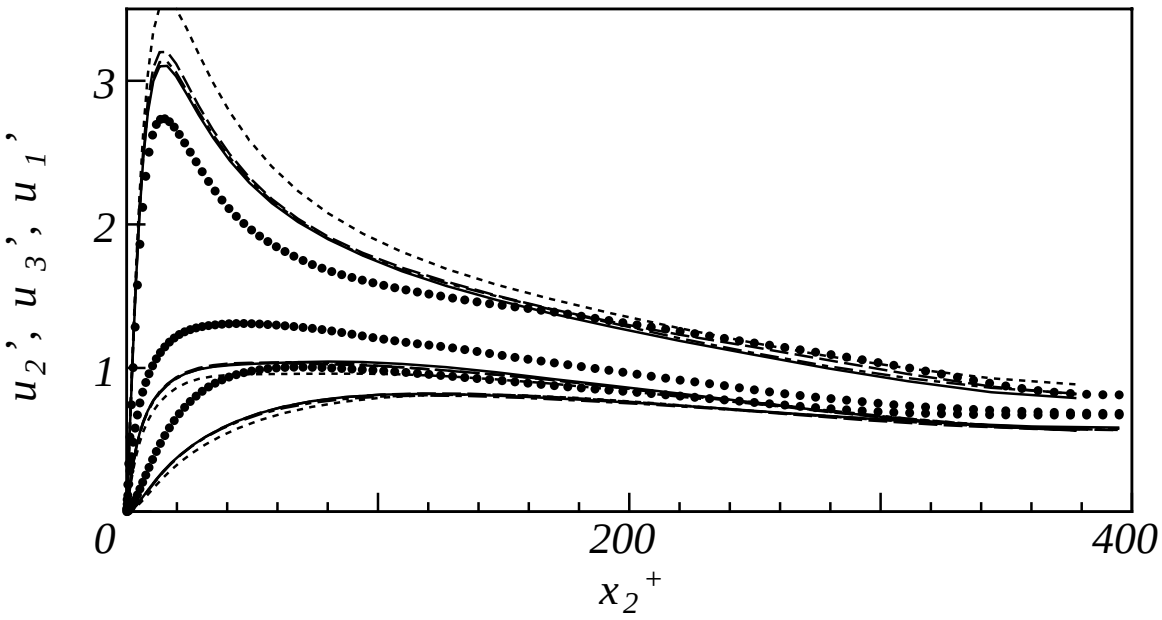

FIGURE 4. Velocity fluctuations of the channel flow at Re_τ =395 using DSM. For symbols see Fig. 3.

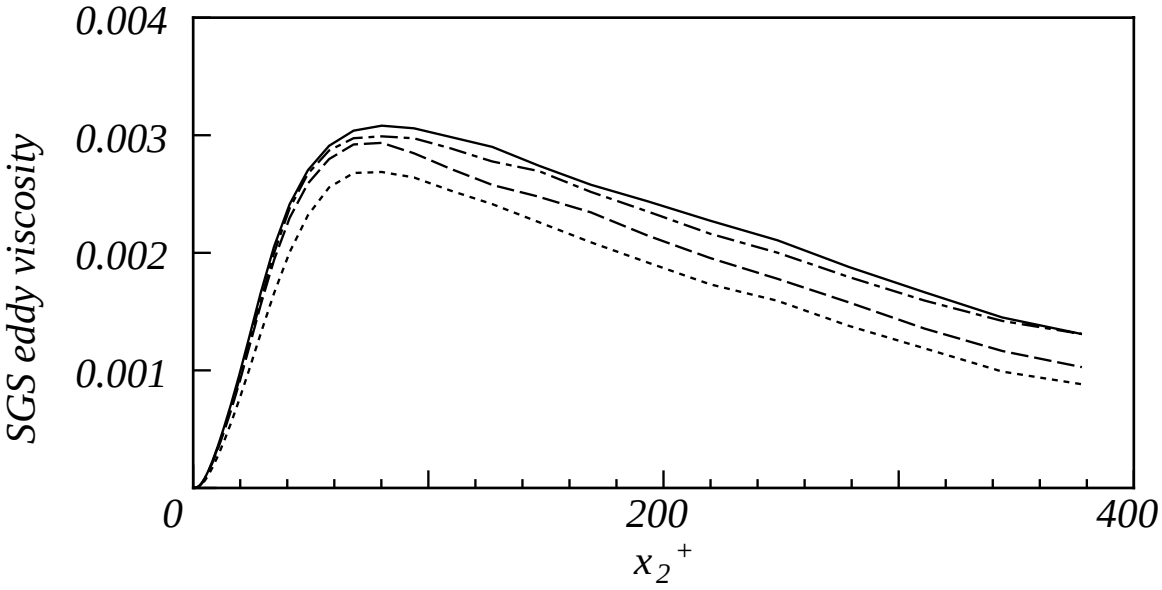

FIGURE 5. SGS eddy viscosity of the channel flow at Re_τ =395 using DSM with the 2nd (·····), 4th (– – – –), 8th (— – —) and 12th (———) order schemes.

assumed as follows.

$$\widehat{\frac{\partial u_i u_j}{\partial x_j}} = \frac{\delta \hat{\bar{u}}_i \hat{\bar{u}}_j}{\delta x_j} + \frac{\partial T_{ij}}{\partial x_j} \tag{12}$$

The model parameter in the dynamic SGS model is determined through the following vector level identity:

$$\mathcal{C}_i = \frac{\partial T_{ij}}{\partial x_j} - \widehat{\frac{\partial \tau_{ij}}{\partial x_j}}, \tag{13}$$

where the resolved convective term $\mathcal{C}_i$ is defined as

$$\mathcal{C}_i = \mathcal{C}_{ij}^j, \qquad \mathcal{C}_{ij}^k = \widehat{\frac{\delta \bar{u}_i \bar{u}_j}{\delta x_k}} - \frac{\delta \hat{\bar{u}}_i \hat{\bar{u}}_j}{\delta x_k}. \tag{14}$$

If the parameter in the dynamic SGS model is estimated through the vector level identity given by Eq. (13), then the numerical error explicitly affect the model parameter. Substituting Eqs. (6) and (7) into Eq. (13), we obtain the following error E_i:

$$E_i = \big(\mathcal{C}_i - \frac{1}{3}\delta_{ij}\mathcal{C}_{kk}^j\big) + 2M_i(C_S\bar{\Delta})^2 + 2M_{ij}\frac{\partial (C_S\bar{\Delta})^2}{\partial x_j}, \tag{15}$$

where

$$M_i = \frac{\partial M_{ij}}{\partial x_j}.$$

The least square minimization of Lilly (1992) is not applicable in this case due to the presence of third term on the right-hand side of Eq. (15). In this study, $(C_S\bar{\Delta})^2$ is estimated by minimizing the following weighted integral:

$$\int\int\int w(x_2)Q(x_1,x_2,x_3)dx_1dx_2dx_3, \tag{16}$$

where $w(x_2)$ is a weight function and $Q = E_iE_i$. Assuming that C_S is a function of x_2 and taking the average in the periodic directions, the $(C_S\bar{\Delta})^2$ value, which minimizes the integral (16), is obtained through the variational principal, which leads to the following differential equation:

$$\begin{aligned} &w(x_2)\Big[\langle \mathcal{C}_i M_i\rangle + 2\langle M_i M_i\rangle (C_S\bar{\Delta})^2 + \langle M_{i2}M_i\rangle \frac{d(C_S\bar{\Delta})^2}{dx_2}\Big] \\ &- \frac{d}{dx_2}\Big[w(x_2)\big(\langle \mathcal{C}_i M_{i2}\rangle + 2\langle M_i M_{i2}\rangle (C_S\bar{\Delta})^2 + \langle M_{i2}M_{i2}\rangle \frac{d(C_S\bar{\Delta})^2}{dx_2}\big)\Big] = 0. \end{aligned} \tag{17}$$

Equation (17) is discretized using the second order finite difference method and is solved using the direct tri-diagonal solver. In this study the weight is selected as $w(x_2) = 1/\Delta_{x_2}(x_2)$, where $\Delta_{x_2}(x_2)$ is the grid spacing in x_2. The dynamic Smagorinsky model given by Eq. (6) with $(C_S\bar{\Delta})^2$ determined by Eq. (17) is called VDSM.

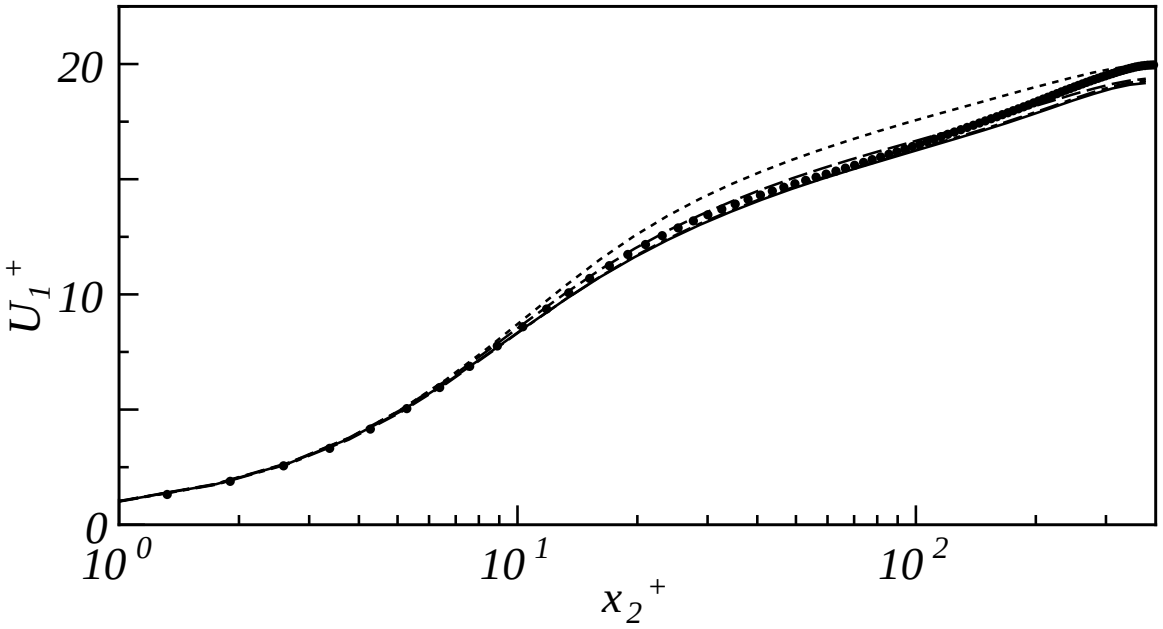

FIGURE 6. Mean streamwise velocity of the channel flow at Re_τ =395 using VDSM with the 2nd (·····), 4th (- - - -), 8th (— - —) and 12th (——) order schemes. DNS (•) data are also plotted.

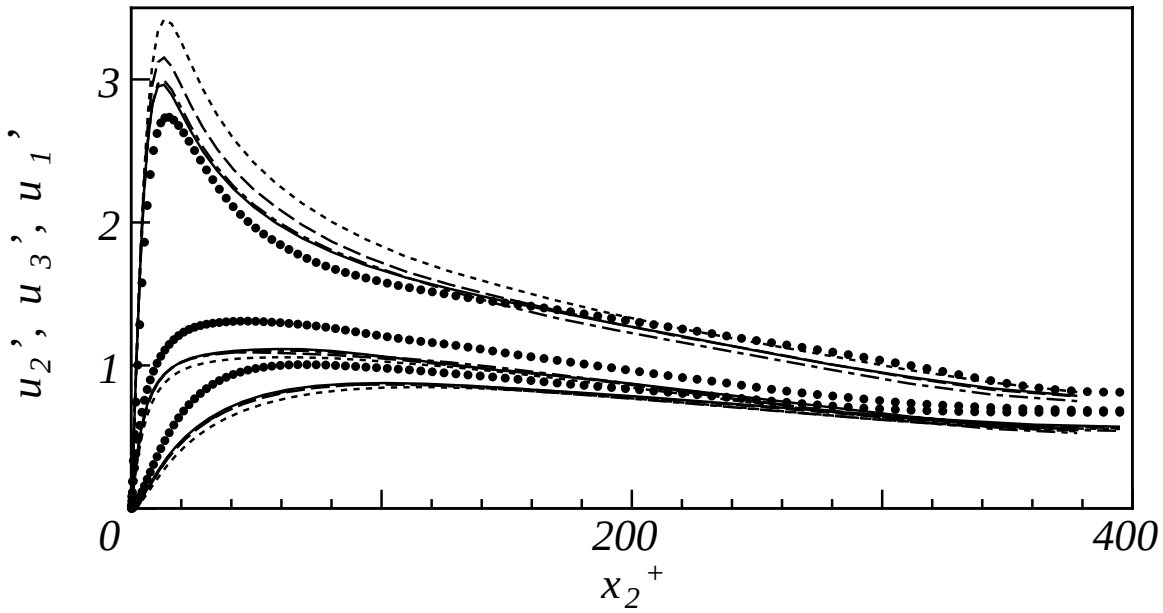

FIGURE 7. Velocity fluctuations of the channel flow at Re_τ =395 using VDSM. For symbols see Fig. 6.

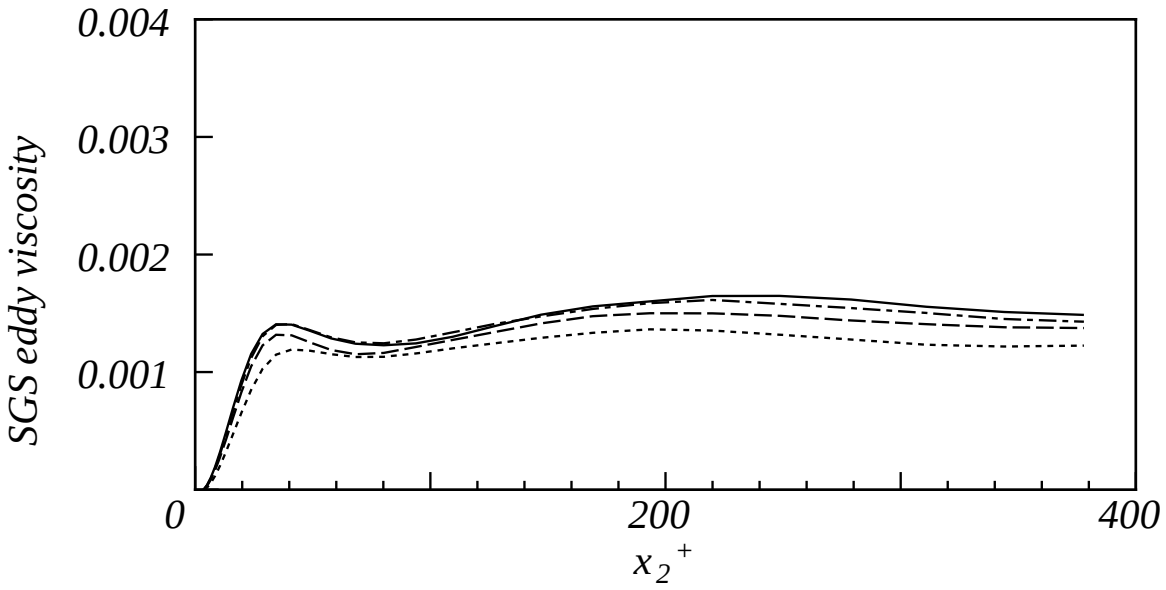

FIGURE 8. SGS eddy viscosity of the channel flow at Re_τ =395 using VDSM with the 2nd (·····), 4th (– – – –), 8th (— — —) and 12th (———) order schemes.

Figures 6, 7, and 8 show the profiles of mean streamwise velocity, velocity fluctuations, and SGS eddy viscosity respectively using the higher order schemes with VDSM at Re_τ=395. Although the mean velocity profile for the second order scheme is still higher than the DNS data, the great improvement is accomplished by using the vector level identity. It is noteworthy that the mean velocity profile in the core region is qualitatively represented by VDSM with the higher order schemes while it is not done by DSM.

Figure 9 shows the profiles of the model parameter C_S using the fourth order scheme with DSM and VDSM at $Re_\tau = 395$. The traditional C_S value with the Van Driest (1956) type wall dumping function, $C_S = 0.1 \times [1 - \exp(-x_2^+/25)]$, is also plotted. Near the wall the C_S profile for VDSM qualitatively coincides with the one for DSM although there exists a slight negative region very near the wall in the profile of VDSM. The peak value of the negative region of C_S is about -0.005, and it has practically no effect on the results of computations. The C_S profile by VDSM differs qualitatively from that by DSM in the region away from the wall, and this is the important difference between the tensor and vector level identities. It appears that the profile of C_S away from the wall is affected strongly by the numerical error. It is interesting that the C_S profile by VDSM is closer to the traditional profile than that by DSM in the buffer region.

2.3 Recommended modification to the dynamic two-parameter mixed model

The dynamic two-parameter mixed model of Salvetti & Banerjee (1995) is based on the scale similarity model of Bardina *et al.* (1983) and the Smagorinsky eddy viscosity model.

$$\tau_{ij}^* = C_L\left(\overline{\bar{u}_i\bar{u}_j} - \bar{\bar{u}}_i\bar{\bar{u}}_j\right)^* - 2(C_S\bar{\Delta})^2|\bar{S}|\bar{S}_{ij} \tag{18}$$

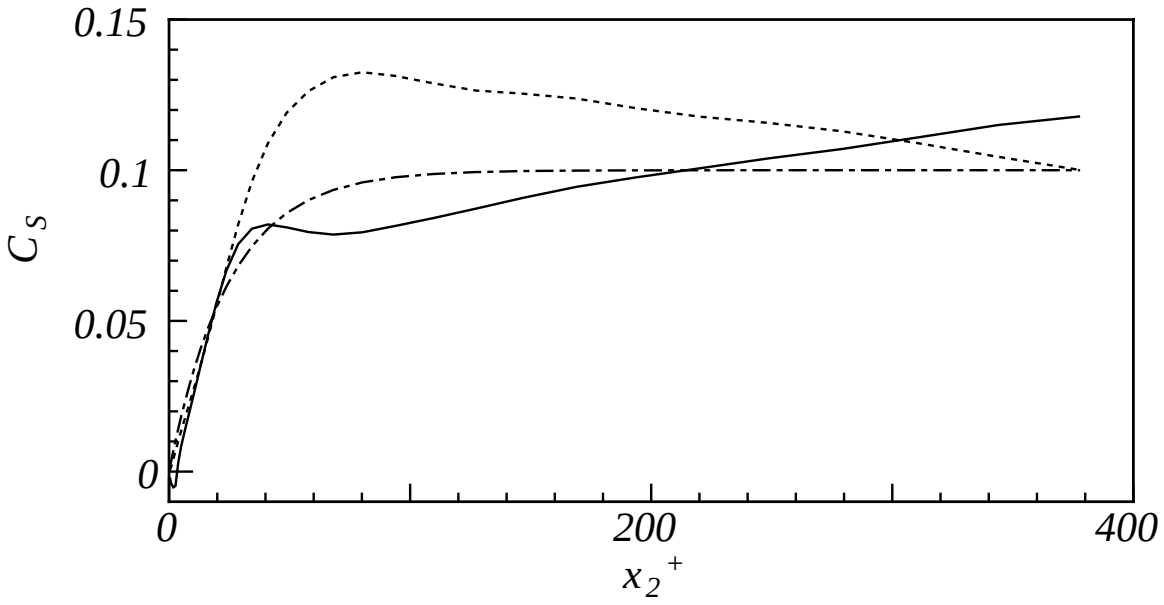

FIGURE 9. The profiles of C_S of the channel flow at Re_τ =395 using DSM (·····) and VDSM (———) with the fourth order scheme. The traditional profile (—-—), $C_S = 0.1 \times [1 - \exp(-\frac{x_2^+}{25})]$, is also plotted.

The scale similarity model by itself is not dissipative enough, and the Smagorinsky eddy viscosity model is usually added to recover the defect. Following the standard procedure for the plane channel flow, the two parameters, C_S and C_L, are computed simultaneously using the tensor level identity of Germano *et al.* (1991) with the least square minimization. The resulting equations for C_S and C_L are given by

$$(C_S\bar{\Delta})^2 = -\frac{1}{2}\frac{\langle \mathcal{L}_{ij}M_{ij}\rangle \langle \mathcal{H}^*_{ij}\mathcal{H}^*_{ij}\rangle - \langle \mathcal{L}_{ij}\mathcal{H}^*_{ij}\rangle \langle \mathcal{H}^*_{ij}M_{ij}\rangle}{\langle M_{ij}M_{ij}\rangle \langle \mathcal{H}^*_{ij}\mathcal{H}^*_{ij}\rangle - \langle \mathcal{H}^*_{ij}M_{ij}\rangle^2}, \tag{19}$$

$$C_L = \frac{\langle \mathcal{L}_{ij}\mathcal{H}^*_{ij}\rangle \langle M_{ij}M_{ij}\rangle - \langle \mathcal{L}_{ij}M_{ij}\rangle \langle \mathcal{H}^*_{ij}M_{ij}\rangle}{\langle M_{ij}M_{ij}\rangle \langle \mathcal{H}^*_{ij}\mathcal{H}^*_{ij}\rangle - \langle \mathcal{H}^*_{ij}M_{ij}\rangle^2}, \tag{20}$$

where

$$\mathcal{H}_{ij} = \left(\widehat{\overline{\hat{\bar{u}}_i\hat{\bar{u}}_j}} - \hat{\bar{\bar{u}}}_i\hat{\bar{\bar{u}}}_j\right) - \left(\widehat{\overline{\bar{u}_i\bar{u}_j}} - \widehat{\bar{\bar{u}}_i\bar{\bar{u}}_j}\right).$$

In this study, the dynamic mixed model given by Eq. (18) with Eqs. (19) and (20) is called DTM.

Figures 10, 11, and 12 show the profiles of mean streamwise velocity, velocity fluctuations, and SGS eddy viscosity respectively using the higher order schemes with DTM at Re_τ=395. The profile of streamwise velocity fluctuation for DTM is better than the one for DSM (compare Fig. 11 with Fig. 4). However DTM has a defect in that the mean velocity profile is lower than that of DNS when it is used with the higher order schemes. Although the mean velocity profile of DTM

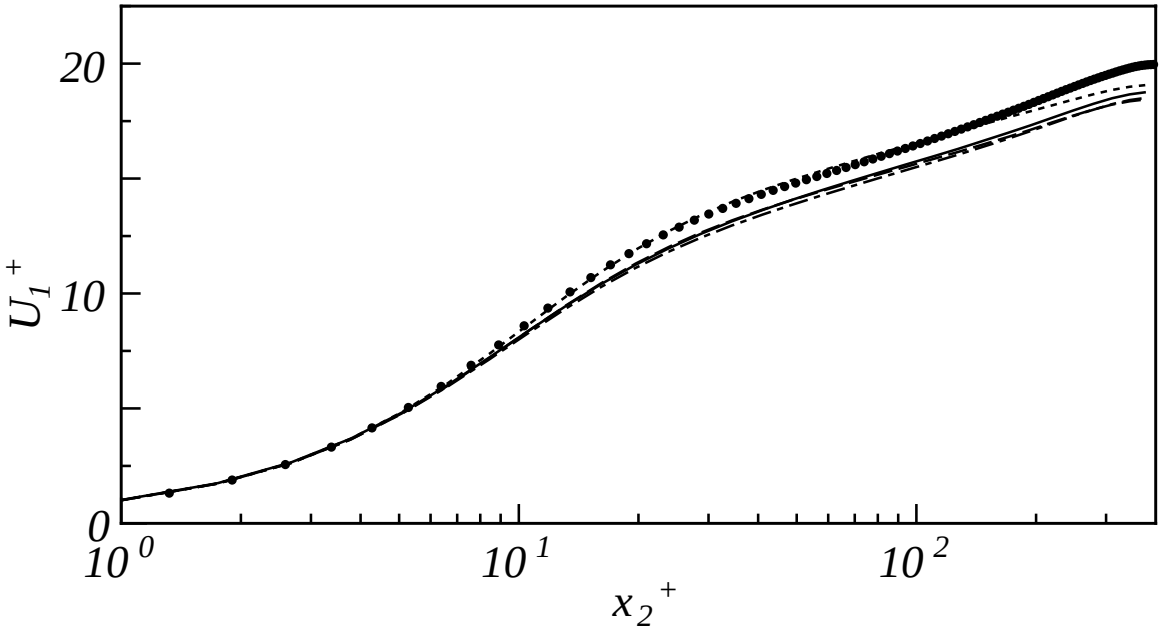

FIGURE 10. Mean streamwise velocity of the channel flow at Re_τ =395 using DTM with the 2nd (·····), 4th (----), 8th (—-—) and 12th (———) order schemes. DNS (•) data are also plotted.

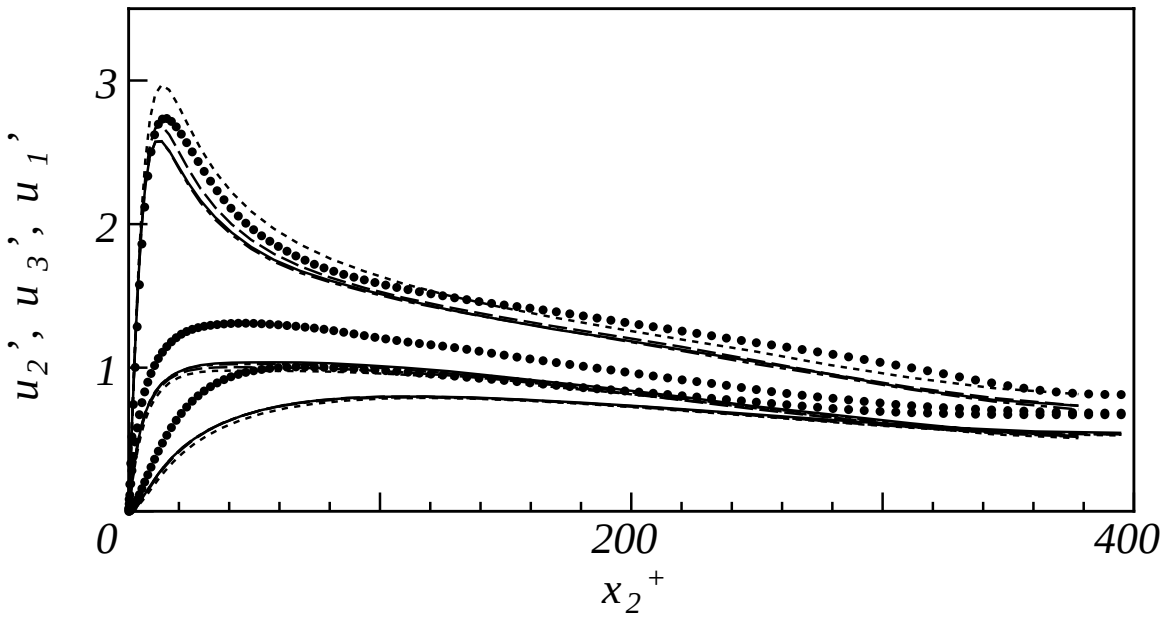

FIGURE 11. Velocity fluctuations of the channel flow at Re_τ =395 using DTM. For symbols see Fig. 10.

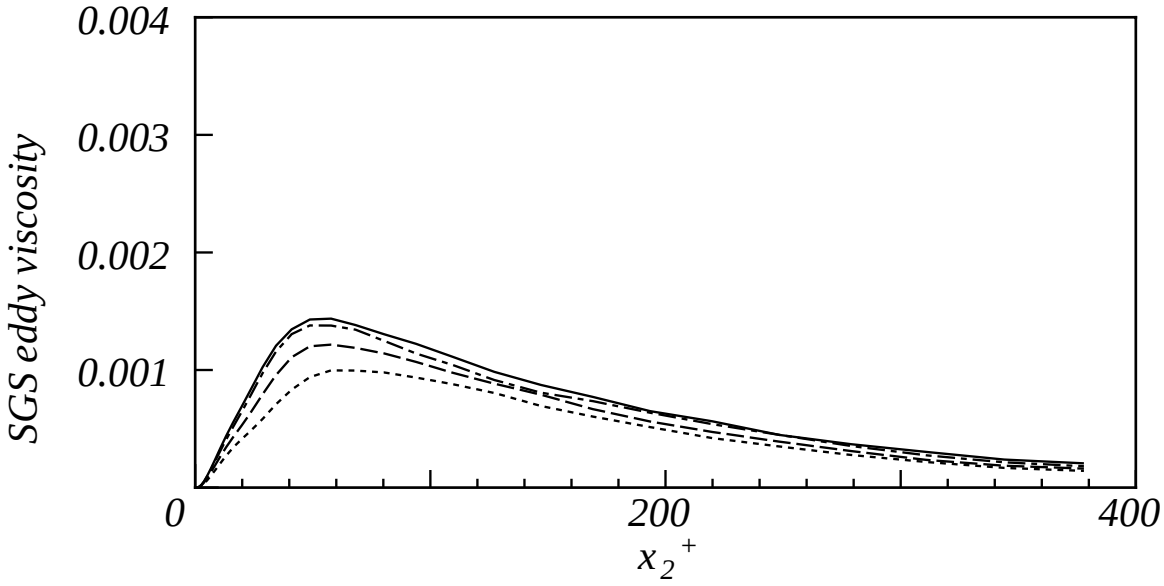

FIGURE 12. SGS eddy viscosity of the channel flow at Re_τ =395 using DTM with the 2nd (·····), 4th (- - - -), 8th (— - —) and 12th (———) order schemes.

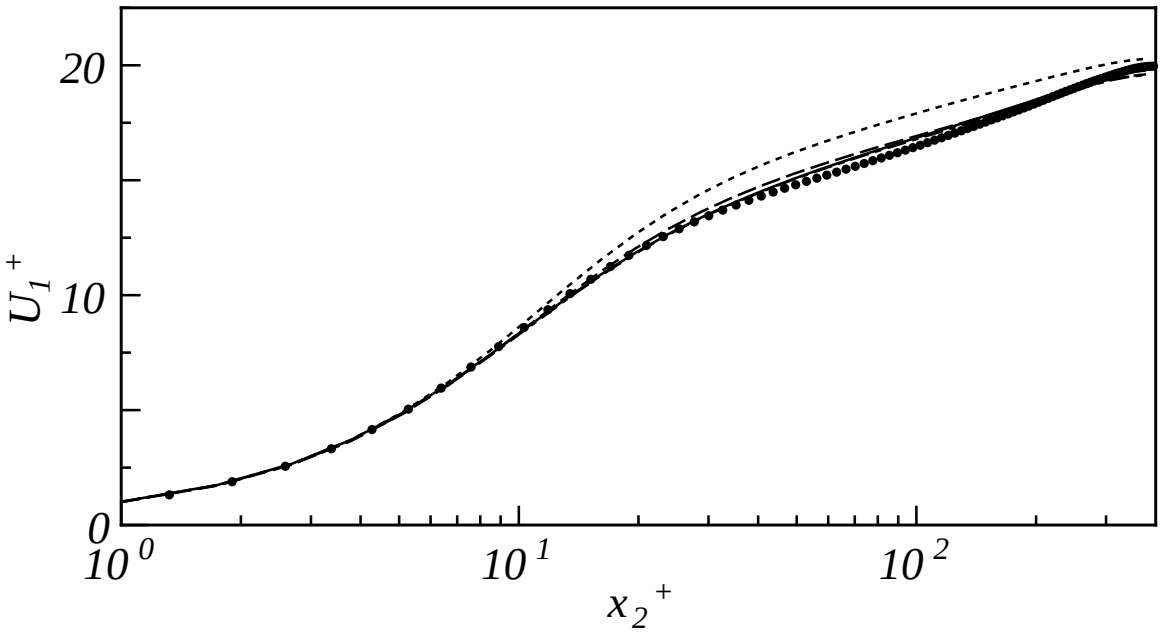

FIGURE 13. Mean streamwise velocity of the channel flow at Re_τ =395 using DTMR with the 2nd (·····), 4th (- - - -), 8th (— - —) and 12th (———) order schemes. DNS (•) data are also plotted.

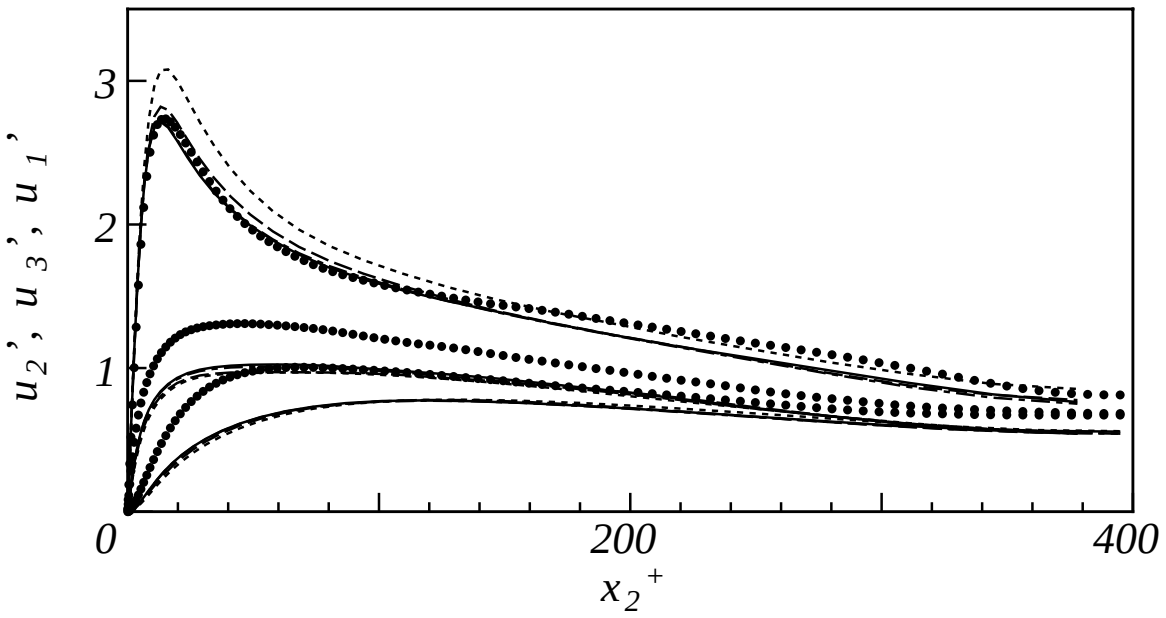

FIGURE 14. Velocity fluctuations of the channel flow at Re_τ =395 using DTMR. For symbols see Fig. 13.

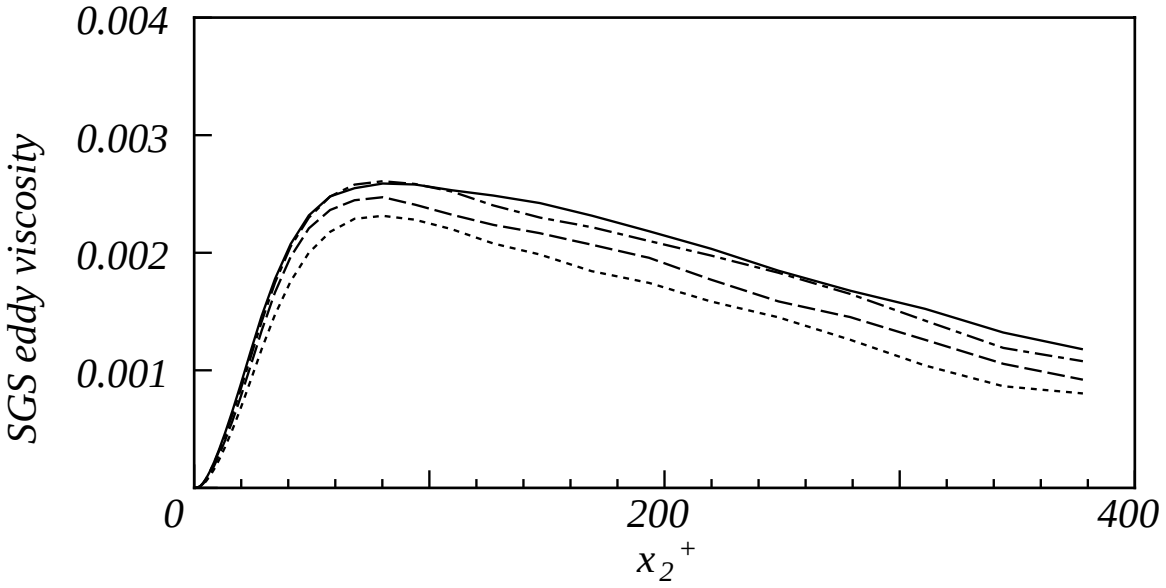

FIGURE 15. SGS eddy viscosity of the channel flow at Re_τ =395 using DTMR with the 2nd (·····), 4th (- - - -), 8th (— — —) and 12th (———) order schemes.

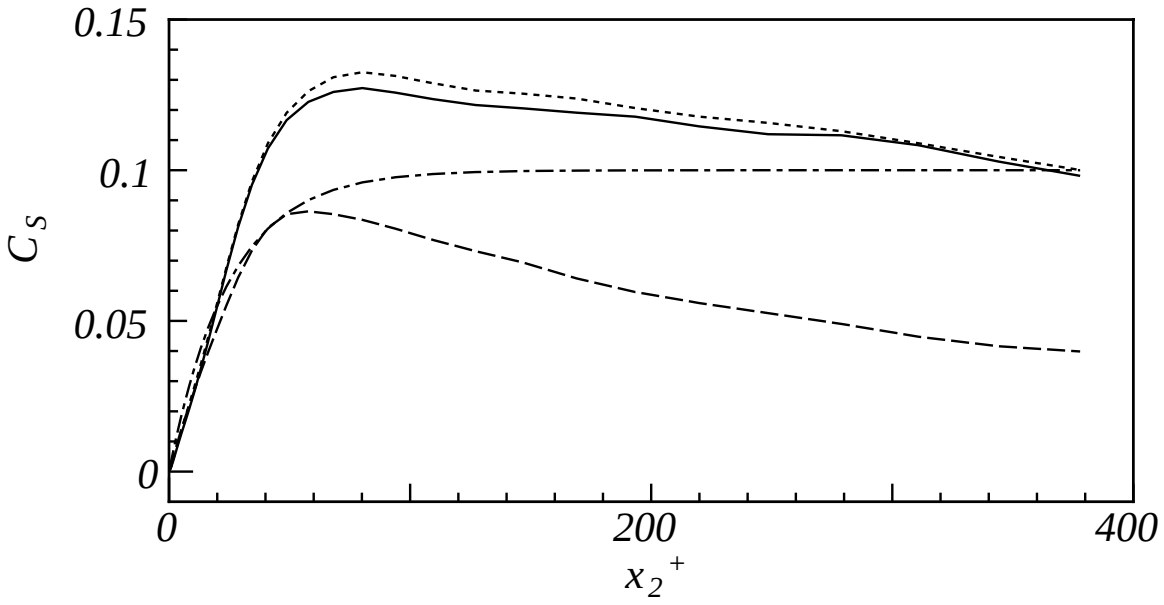

FIGURE 16. The profiles of C_S of the channel flow at Re_τ =395 using DSM (⋯⋯), DTM (- - - -) and DTMR (———) with the fourth order scheme. The traditional profile (—·—), $C_S = 0.1 \times [1 - \exp(-\frac{x_2^+}{25})]$, is also plotted.

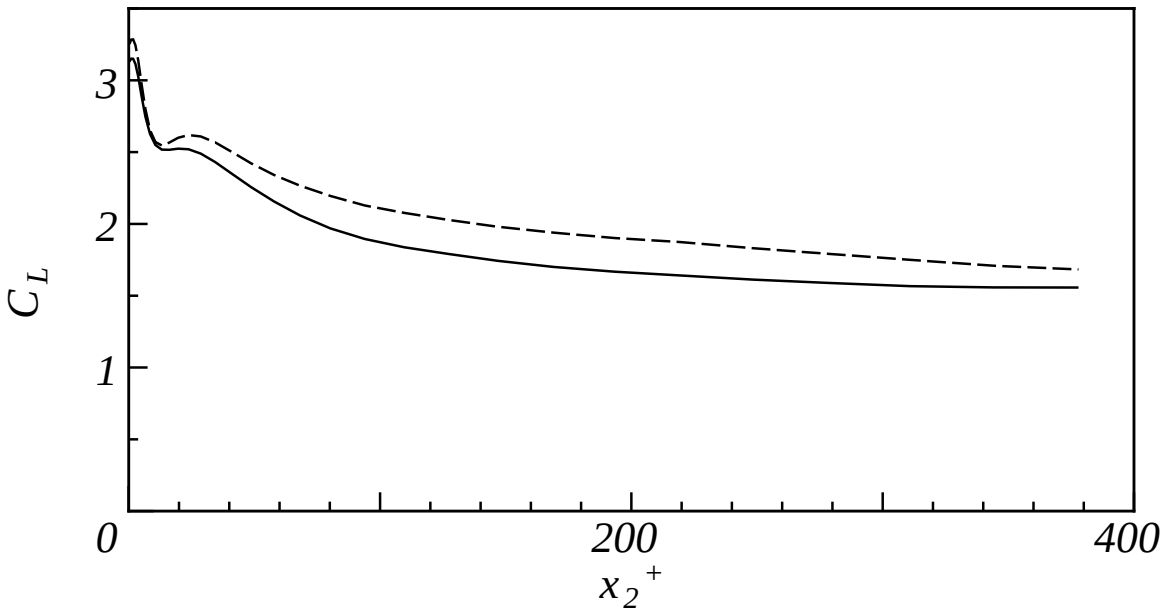

FIGURE 17. The profiles of C_L of the channel flow at Re_τ =395 using DTM (- - - -) and DTMR (———) with the fourth order scheme.

with the second order finite difference method accidentally agrees well with the DNS data, it is caused by the numerical error explained in Fig. 1. In this stage, the model parameters in DTM are estimated through the tensor level identity, and the numerical error is not taken into consideration. Remember that the scale similarity model itself has less dissipation, and therefore the model is used together with the Smagorinsky model as the mixed model to remove the defect. However the profiles of the SGS eddy viscosity in Fig. 12 are much smaller than those in Fig. 5. This indicates that the defect of the scale similarity model is not cured if the model parameters are estimated through the dynamic procedure with the tensor level identity. The reason why the defect is not cured is that the correlation of the Smagorinsky model to the SGS stress is much lower than that of the scale similarity model (for example see Horiuti 1989). This imbalance makes C_S smaller if the two parameters are solved simultaneously.

To remove the problem, Morinishi (1997) proposed a modification to a dynamic two-parameter mixed model. First, the Smagorinsky parameter C_S is computed exactly the same way as in DSM (using Eq. (9)). This ensures that the mixed model has enough dissipation. Secondly, the other parameter is computed dynamically as C_S is known. In this study, we adopt the following modification to the mixed model (18):

$$C_L = \frac{\left\langle [\mathcal{L}_{ij} + 2(C_S\bar{\Delta})^2 M_{ij}]\mathcal{H}^*_{ij} \right\rangle}{\left\langle \mathcal{H}^*_{ij}\mathcal{H}^*_{ij} \right\rangle}. \tag{21}$$

This revised dynamic two-parameter mixed model is called DTMR.

Figures 13, 14, and 15 show the profiles of mean streamwise velocity, velocity fluctuations, and SGS eddy viscosity respectively using the higher order schemes with DTMR at Re_τ=395. The profiles of the mean velocity and velocity fluctuation using the higher order schemes with DTMR coincide well with the DNS data. Comparing Fig. 15 with Fig. 12, it is apparent that the defect of DTM is recovered by the revised model. Figures 16 and 17 show the profiles of the parameters C_S and C_L respectively by the fourth order scheme with DTM and DTMR (and DSM in Fig. 16). The traditional C_S value with the wall dumping function is also plotted in Fig. 16. The C_S profile of DTMR is almost the same as that of DSM, and the merit of DSM is kept in DTMR. The C_S value of DTM is much lower than those of DSM, DTMR, and the traditional value, and this makes DTM less dissipative. The C_L profile of DTMR is almost the same as that of DTM, and the merit of DTM is kept in DTMR.

3. Future plans

The proposed SGS models will be tested in high Reynolds number channel flow to see if they work well in LES for practical problems. In addition, the vector level identity will be extended to the revised two-parameter mixed model.

REFERENCES

Bardina, J., Ferziger, J. H. & Reynolds, W. C. 1983 Improved turbulence models based on large eddy simulation of homogeneous, incompressible, turbulent flows, Stanford University Tech. Rep. TF-19.

Dukowicz, J. K. & Dvinsky, A. S. 1992 Approximation as a higher order splitting for the implicit incompressible flow equations. *J. Comput. Phys.* **102,** 336-347.

Germano, M., Piomelli, U., Moin, P. & Cabot, W.H. 1991 A dynamic subgrid-scale eddy viscosity model. *Phys. Fluids A.* **3,** 1760-1765.

Ghosal, S. 1996 An analysis of numerical error in large-eddy simulation of turbulence. *J. Comput. Phys.* **125,** 187-206.

Horiuti, K. 1989 The role of the Bardina model in large eddy simulation of turbulent channel flow. *Phys. Fluids A.* **1,** 426-428.

Horiuti, K. 1997 A new dynamic two-parameter mixed model for large-eddy simulation. *Phys. Fluids A.* **9,** 3443-3464.

Mansour, N. N., Moser, R. D. & Kim, J. 1996 Reynolds number effects in low Reynolds number turbulent channels. (In preparation, data in AGARD database.)

Morinishi, Y. 1997 Large eddy simulation of plane channel turbulence using dynamic two-coefficient mixed subgrid-scale models. *Trans. JSME.* **63-606B,** 529-536 (*in Japanese*).

Morinishi, Y., Lund, T.S., Vasilyev, O. V. & Moin, P. 1998 Fully conservative higher order finite difference schemes for incompressible flow. *J. Comput. Phys.* **143,** 90-124.

Rodi, W. & Mansour, N. N. 1993 Low-Reynolds-number $\kappa - \epsilon$ modeling with the aid of direct simulation data. *J. Fluid Mech.* **250,** 509-529.

Salvetti, M. & Banerjee, S. 1995 A priori tests of a new dynamic subgrid-scale model for finite-difference large-eddy simulations. *Phys. Fluids A.* **7,** 2831-2847.

Smagorinsky, J. 1963 General circulation experiments with the primitive equations. I. The basic experiment. *Mon. Weather Rev.* **91,** 99-165.

Spalart, P., Moser, R. & Rogers, M. 1991 Spectral methods for the Navier-Stokes equations with one infinite and two periodic direction. *J. Comput. Phys..* **96,** 297-324.

Van Driest, E.R., H. 1956 On turbulent flow near a wall. *J. Aero. Sci.* **23,** 1007-1011,1036.

Vreman, B., Geurts, B. & Kuerten, H. 1994 On the formulation of the dynamic mixed subgrid-scale model. *Phys. Fluids A.* **6,** 4057-4059.

Zang, Y., Street, R. L. & Koseff, J. R. 1993 A dynamic subgrid-scale model and its application to turbulent recirculating flows. *Phys. Fluids A.* **5,** 3186-3196.